PROCEEDINGS of ISMA 2019
International Symposium on Music Acoustics

13 - 17 September 2019 in Detmold, Germany

Numerical study of synchronization phenomena of an air-jet instrument using finite-difference lattice boltzmann method

Ryoya Tabata[(1)], Taizo Kobayashi[(2)], Kin'ya Takahashi[(3)]

[(1)]Kyushu Institute of Technology, Japan, tabata@chaos.mse.kyutech.ac.jp
[(2)]RIIT, Kyushu University, Japan, tkoba@cc.kyushu-u.ac.jp
[(3)]Kyushu Institute of Technology, Japan, takahasi@mse.kyutech.ac.jp

Abstract

In this study, we focus on the synchronization between an air-jet instrument and external sound source. We numerically explore the synchronization mechanism using a finite-difference lattice Boltzmann method (FDLBM) as a direct aeroacoustic simulation scheme in two dimensions. We succeed in reproducing the frequency-locking phenomenon between the monopole sound source and air-jet instrument in the stationary state. Numerical simulations are conducted on a GPU cluster to explore the large parameter space. Transient behavior towards the frequency-locking phenomenon was observed, and the results demonstrate that the external sound source strongly affects the air-jet oscillation and the phase relationship of the sound pressure inside the resonator.

Keywords: Air-jet instrument, Synchronization, Aeroacoustic simulation

1 INTRODUCTION

A flue organ pipe is an air-jet instrument whose sound source is an aerodynamic sound generated by an air jet impinging on a wedge-shaped object. A feedback mechanism occurs between the air jet and a resonance tube, owing to the influence of the sound pressure in the resonance tube on the air jet.

When two organ pipes with pitches that are close to each other stand abreast, the frequency-locking phenomenon and oscillation death (quenching) occur, as first mentioned by Lord Rayleigh [1]. To study the synchronization mechanism among flue organ pipes, coupled Van der Pol oscillators [2, 3] are often used. Fischer et al. [2] suggested that the effect of the near-field interaction between the air-jet motion and acoustic field plays an important role in the synchronization mechanism. The synchronization characteristics of Van der Pol model are usually analyzed by relying on synchronization theory [4, 5]. Okada et al. [5] showed that the van der Pol oscillator cannot cause higher-order locking because its infinitesimal phase response curve (iPRC) hardly has any higher Fourier components. To improve the model, it is important to investigate the complex dynamics of the air-jet instrument in the synchronization regime.

A compressible flow simulation has been employed to reproduce the sound vibration of an air-reed instrument [6, 7, 8, 9], and the lattice Boltzmann method (LBM) has been employed as an alternative method to the Navier–Stokes equations owing to its advantage of a simple implementation on many-core accelerators such as GPU [6, 9]. The standard LBM only has second-order accuracy in both the spatial and temporal dimensions, and is not sufficiently accurate for direct aeroacoustic simulations [10]. Furthermore, the LBM is unstable in the high Mach number regime, even with the use of the multiple relaxation time (MRT) model [9]. In contrast, since the finite-difference lattice Boltzmann method (FDLBM) [11] can utilize finite-difference schemes of arbitrary order, it is capable of simulating numerical models stably and efficiently.

In this study, we employ the FDLBM to numerically investigate the synchronization mechanism between an air-jet instrument and external sound source. This paper is structured as follows. In Section 2, we introduce the numerical procedure utilized in this study. In Section 3, the numerical simulation is verified on several benchmark problems. In Section 4, we first discuss the behavior of the air-jet instrument for several air-jet velocities without a sound source. Then, we discuss the synchronization mechanism with a sound source with a varying frequency. Finally, Section 5 provides a discussion of the results and suggestions for future work.

2 NUMERICAL PROCEDURE

2.1 Governing equation and discretization

In this study, we employ the FDLBM model proposed by Tsutahara [11] with the added monopole sound source term proposed by Viggen [12]. The discrete Boltzmann equation (DBE) with a collision term (the third term of the left-hand side) added for numerical stability and the sound source term s_i can be respectively written as

$$\frac{\partial f_i}{\partial t} + \mathbf{c}_i \frac{\partial f_i}{\partial \mathbf{x}} - \frac{A\mathbf{c}_i}{\tau} \frac{\partial (f_i - f_i^{(0)})}{\partial \mathbf{x}} = s_i - \frac{1}{\tau}[f_i - f_i^{(0)}], \tag{1}$$

$$s_i(\vec{x},t) = w_i A_0 \sin(\omega t) exp(\frac{-ln2(\vec{x}-\vec{x}_0)^2}{b^2}). \tag{2}$$

The dispersion-relation-preserving (DRP) scheme [13], or third-order upwind scheme (UTOPIA), is employed for space discretization, and the second-order Runge–Kutta method is employed for time evolution. When using the DRP scheme, artificial selective damping [14] is used to suppress waves with small wavelengths.

Using the D2Q9 model [15], the numerical simulations were performed on the GPU (Tesla P100) cluster of ITO subsystem B (RIIT, Kyushu Univ) using an efficient GPU implementation [16].

2.2 Computational domain and air-jet instrument model

Figure 1 depicts the computational domain of the numerical simulation for reproducing the synchronization between an air-jet instrument and monopole sound source. Figure 2 illustrates the air-jet instrument model employed in this study, with two sampling points displayed in the figure. The characteristic length L is the nozzle width of the air-jet instrument. The non-uniform mesh was constructed by gradually increasing the mesh size of the air-jet region, where the smallest mesh was set as Δy = 0.01 (mm).

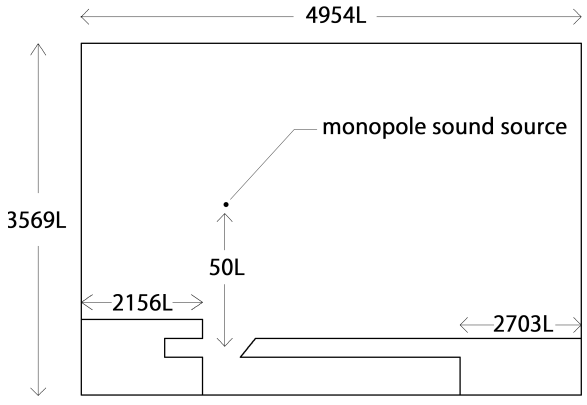

Figure 1. Computational Domain

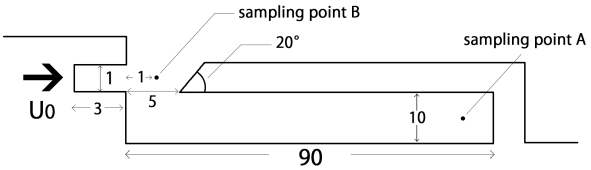

Figure 2. Air-jet instrument model (unit: mm)

2.3 Boundary conditions and initial conditions

An extrapolation method [17] that provides the distribution functions at the boundary by extrapolating using the distribution functions at the adjacent lattice points is employed for the solid boundary. Furthermore, an equilibrium function calculated by zero-order extrapolation of the macroscopic variables is set at the outlet boundary. At the inlet of the air-jet instrument model, the inflow condition is set using a sigmoid function to adjust the flow speed, which reaches the maximum value at t = 0.001 (s).

3 VERIFICATION OF THE NUMERICAL METHOD

3.1 Lid-driven cavity flow

In this subsection, we discuss the accuracy of the numerical method using simulation data provided by Ghia [18] for the 2D lid-driven cavity flow problem. The Reynolds number of the flow is set to 100, with $U_0 = 0.1$. The Zou–He boundary condition [15] is adopted for the LBM calculations. The FDLBM calculations are all performed using a mesh of size 101×101. The following convergence criterion is adopted with ε = 1e-6:

$$\sqrt{\frac{\sum_i |\vec{u}(\vec{x}_i, t^n) - \vec{u}(\vec{x}_i, t^{n-1})|^2}{\sum_i |\vec{u}(\vec{x}_i, t^n)|^2}} < \varepsilon. \tag{3}$$

Figure 3 shows that the FDLBM calculation exhibits a good agreement with Ghia's data. Furthermore, we observe that the LBM calculation gradually approaches Ghia's data as the mesh size increases. This indicates that the FDLBM is capable of calculating the flow more precisely compared with the LBM when the same mesh size is employed.

3.2 2D acoustic pulse propagation

As a typical benchmark problem in computational acoustics, the propagation of a two-dimensional Gaussian pulse simulation is performed. The analytical solution, which can be obtained by solving the linearized Euler equations using the Fourier-Bessel transform [13], is as follows:

$$p'(r,t) = \frac{p_0}{2\alpha} \int_0^\infty \exp\left(-\frac{\xi^2}{4\alpha}\right) \cos(c_s \xi t) J_0(\xi r) \xi d\xi, \tag{4}$$

where $J_0(\xi r)$ is the zeroth-order Bessel function of the first kind. The parameters are set as $p_0 = 0.001$ and $\alpha = 10^2/ln2$. Figure 4 demonstrates a good agreement between the analytical solution and the numerical results obtained by the LBM and FDLBM. The good performance of the LBM can be explained by the fact that the LBM achieves a perfect shift solution for the streaming step. Furthermore, we can observe that the FDLBM performs better when utilizing a high-order scheme.

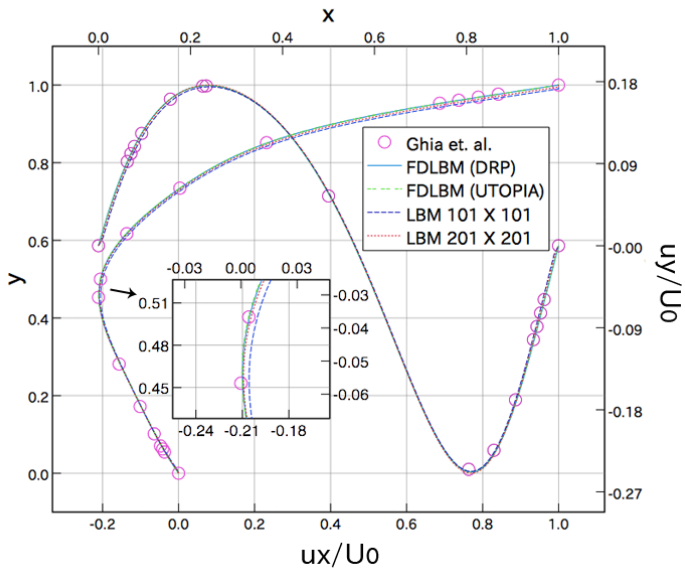

Figure 3. Lid-driven cavity

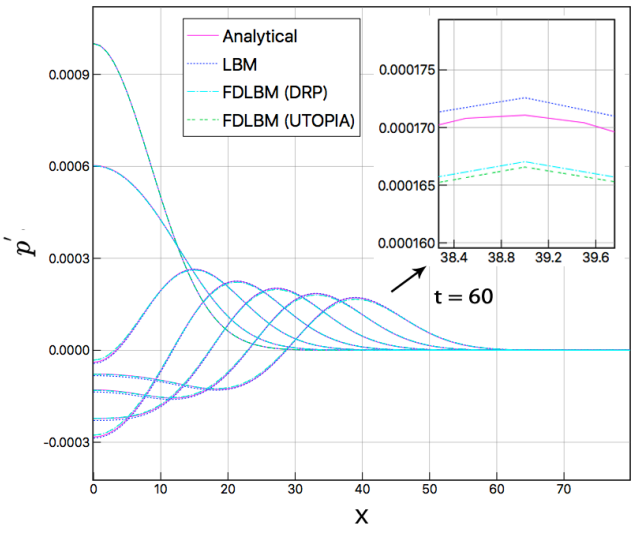

Figure 4. Two-dimensional pulse propagation

4 RESULTS AND DISCUSSIONS

4.1 Simulation without external sound source

In this subsection, we discuss the changes in characteristic frequencies of the sound waves excited in the pipe with an increasing air-jet velocity. Table 1 presents the parameter values adopted in the simulations, which were calculated for up to 0.05 s. For stable calculations, the third-order upwind scheme is adopted for the space discretization. Figure 5 depicts the velocity distributions in the near field of the air-jet instrument model, and Figure 6 shows the pressure fluctuation ($\Delta p = \frac{p-p_0}{p_0}$) distributions in the far field of the calculation domain at time 0.025 s, i.e., the stationary condition, for two inflow velocities (U = 10 m/s, 24 m/s). We can observe that the jet is oscillating and the sound wave is radiating out from the mouth of the air-jet instrument.

Table 1. Parameter values

Parameters	Values
Inflow velocity	U = 6 (m/s) $\sim$ 40 (m/s)
Initial flow density	ρ_0 = 1.184 (kg/m^3)
Coefficient of viscosity	μ = 1.846 $\times$ 10^{-5} (Pa $\cdot$ s)
Sound speed	c_s = 346.18 (m/s)
Time step	Δt = 8.3e-9 (s)
Minimum mesh size	Δy = 0.01 (mm)

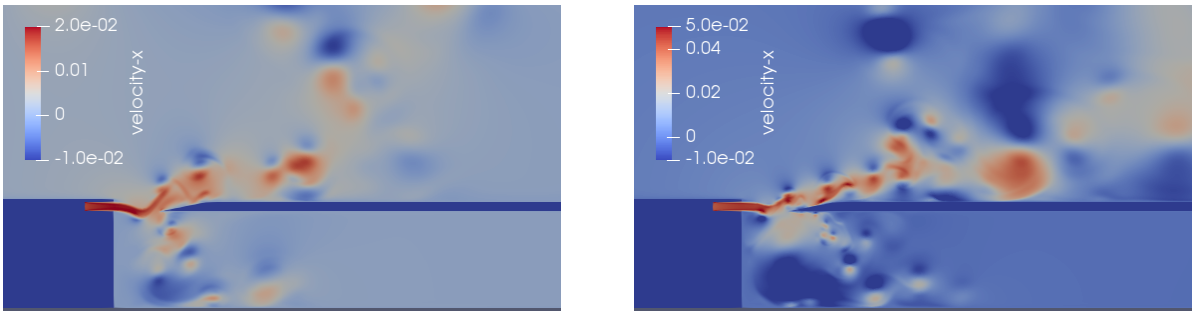

(a) 10 (m/s) (b) 24 (m/s)

Figure 5. Near field velocity distribution (0.025 s)

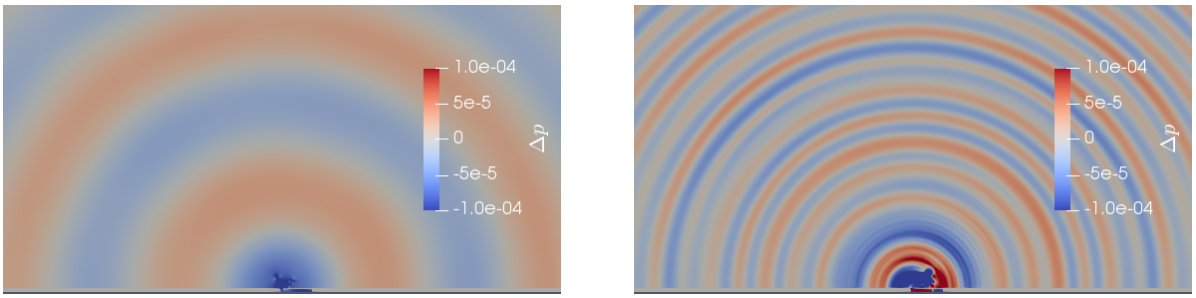

(a) 10 (m/s) (b) 24 (m/s)

Figure 6. Far field pressure fluctuation distribution (0.025 s)

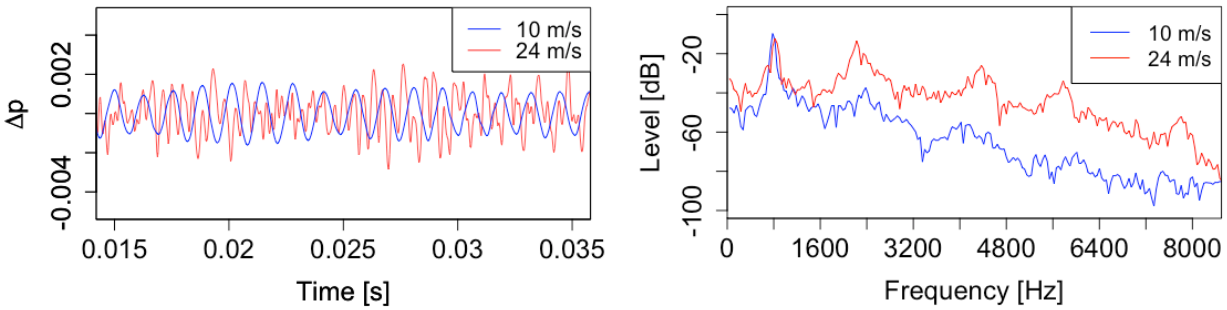

(a) Pressure fluctuations

(b) Power spectra

Figure 7. Pressure fluctuations and power spectra at the pipe end of the instrument

Figure 7a depicts the pressure fluctuations at the pipe end (sampling point A) of the air-jet instrument for the two inflow velocities. A stable oscillation is observed at U =10 m/s, and a slightly unstable oscillation with amplitude modulations is observed at U =24 m/s. Figure 7b depicts the power spectra of the pressure fluctuations. In calculating the spectra, the initial transient oscillation (t < 0.02 s) is omitted. The main peaks of the spectra for U =10 m/s and U = 24 m/s appear at $f = 784$ Hz and $f = 844$ Hz, respectively. The second peak of the spectrum for U = 24 m/s occurs at $f = 2244$ Hz. These results can be explained by the edge tone frequency, the pipe fundamental resonance frequency at $f = 900$ Hz, and the second resonance peak (the third harmonic) at $f = 2755$ Hz, respectively [7]. Brown introduced a semi-empirical equation based on the experimental results, which predicts the frequency of the edge tone [19]:

$$f = 0.466(100U - 40)(\frac{1}{100h} - 0.07), \tag{5}$$

where U denotes the speed of the air jet and h is the distance between the flue and edge. From Figure 8, it can be observed that our numerical result is in good agreement with the predicted edge tone frequency in some ranges of the jet velocity, and it also reproduces the frequency locking to the fundamental and third harmonic resonances of the pipe.

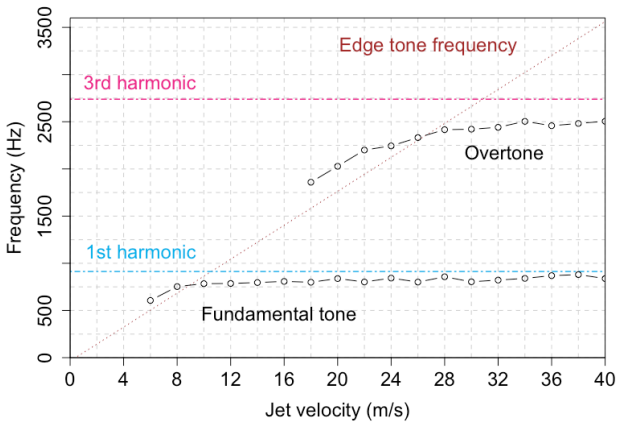

Figure 8. Changes in oscillation frequencies with air jet velocity

4.2 Simulation with an external sound source

In this subsection, we discuss the behavior of the synchronization transition between the air-jet instrument and an external monopole sound source. The inflow velocity of the air-jet instrument is set as $U = 10$ m/s, where the stable oscillation is observed. The sound source strength is set as $A_0 = 3.3 \times 10^{-5}$, which reproduces the same order in pressure fluctuation at the sampling point A as the instrument driven by a jet of 10 m/s.

The frequency of the sound source is set as f =700∼910 Hz with a 2-Hz interval. The sound source is incorporated at t =0.0125 s, where the stable oscillation begins.

Figure 9 depicts the pressure fluctuations at the pipe end (sampling point B) for three cases: the jet driven instrument with a sound source of 796 Hz, that without a sound source, and the case with a sound source but no jet driving. For the case with the sound source, after a short disturbance, we can observe phase locking between the sound source and the pipe end pressure fluctuation. Furthermore, the amplitude of the pressure fluctuation with the sound source becomes greater than that in the case with no sound source in the course of the time evolution.

Figure 10 compares the velocity in the y-direction at the pipe opening (sampling point A) for the cases with and without a sound source. A large velocity fluctuation is observed before the start of the synchronization, as shown in Figure 9. After the synchronization, the amplitude of the velocity fluctuation with the sound source becomes stable, and is greater than that without a sound source.

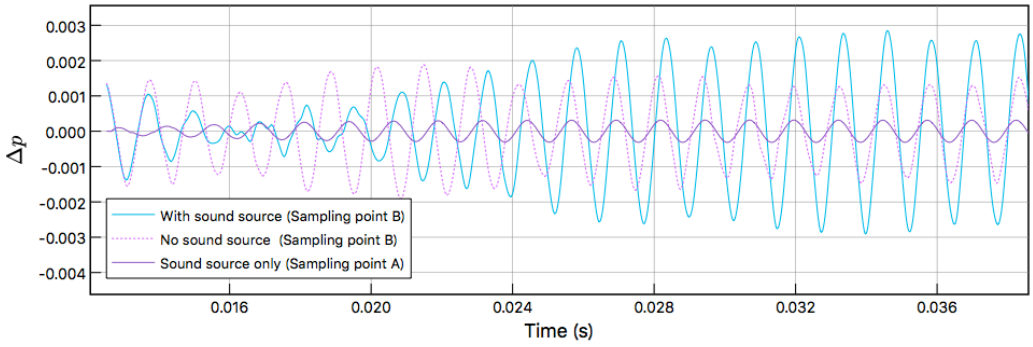

Figure 9. Pressure fluctuations at the pipe end

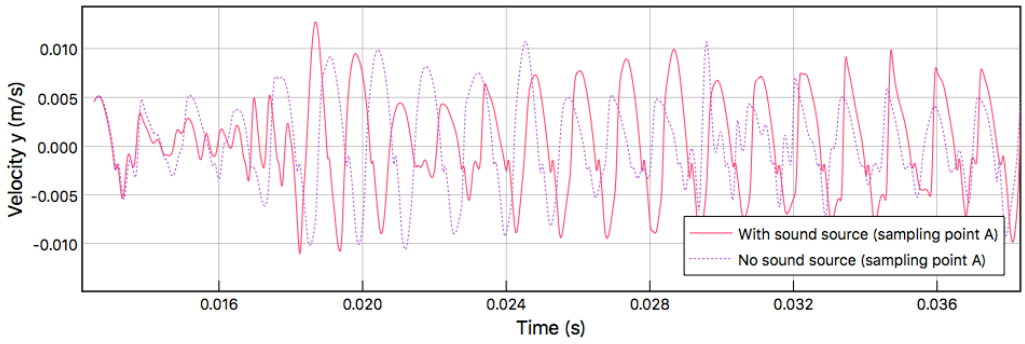

Figure 10. Velocity (y-direction) at the mouth opening of the pipe

Figure 11 illustrates the pressure and velocity distributions for the calculation with the sound source (796 Hz) at 0.054 s. From Figure 11a, the interference between the sound source and the radiated sound from the pipe can be observed. As shown in Figure 11b, a large jet oscillation is observed, which is amplified by the synchronization with the external sound source.

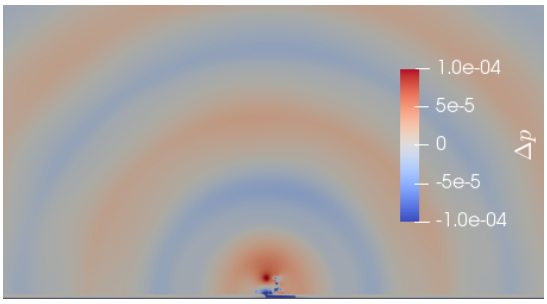

(a) Pressure distribution

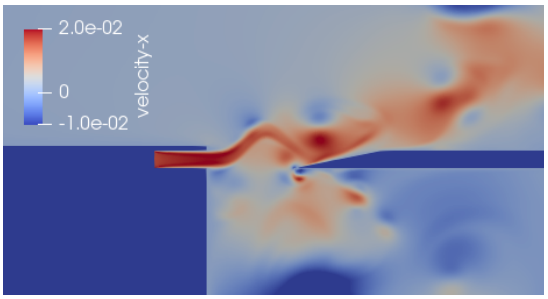

(b) Velocity distribution

Figure 11. Snapshots at t = 0.054 (s) of calculation with sound source (796 Hz)

Figure 12 depicts the power spectra of the pressure fluctuations of the pipe end, and Figure 13 illustrates the pressure fluctuation level at the mouth opening in the plane of the frequency f versus the frequency detuning Δf (in Hz). As observed from these figures, the main peak frequency increases as the external sound source frequency increases. However, out of the approximately range of 730 $\sim$ 830 Hz, the synchronization is broken and the main peak is separated into two peaks: the own-mode frequency of the instrument and external sound source frequency.

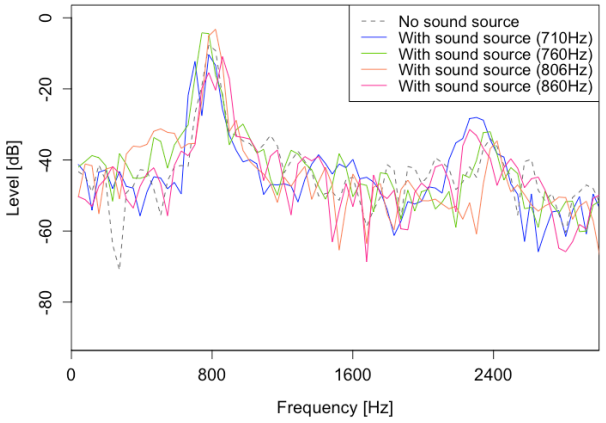

Figure 12. Power spectra at the pipe bottom

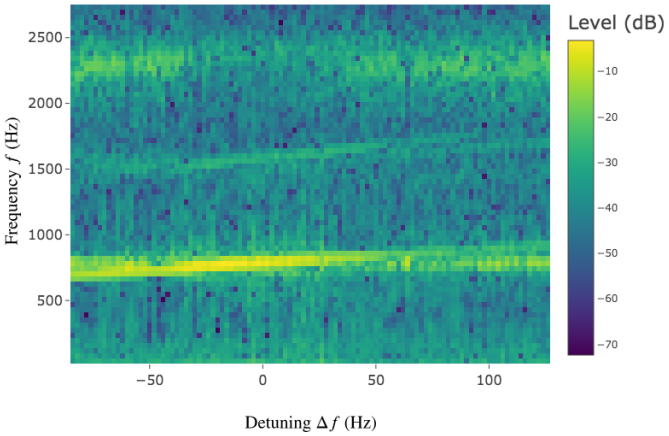

Figure 13. The pressure fluctuation level (in relative dB) in the plane of frequency f versus frequency detuning Δf (in Hz)

5 CONCLUSIONS

In this paper, we have presented the results of numerical simulations of an air-jet instrument using the FDLBM. We found that the FDLBM can reproduce the basic characteristics of the flue instrument and the synchronization between the oscillation mode and an external sound source. Transient behavior towards this synchronization was observed, and it was demonstrated that the external sound source strongly affects the jet oscillation and the phase of the pressure fluctuation. As future work, a three-dimensional simulation should be performed to reproduce more realistic synchronization phenomena between the air-jet instruments.

ACKNOWLEDGEMENTS

This work was supported by JST CREST Grant Number JPMJCR1501, “Joint Usage/Research Center for Interdisciplinary Large-Scale Information Infrastructures” and “High Performance Computing Infrastructure” in Japan (Project IDs: jh190039-ISH and jh190010-MDH). The authors are very grateful to Mr. Sho Iwagami (Kyushu Institute of Technology) for useful discussions.

REFERENCES

[1] J. Rayleigh. *The Theory of Sound*. Vol.2. New York: Dover; 1945. p. 221-222.

[2] Fischer JL, Bader R, Abel M. Aeroacoustical coupling and synchronization of organ pipes. The Journal of the Acoustical Society of America. 2016 Oct;140(4):2344-51.

[3] Sawicki J, Abel M, Schöll E. Synchronization of organ pipes. Eur Phys J B. 2018 Feb 5;91(2):24.

[4] Abel M, Bergweiler S, Gerhard-Multhaupt R. Synchronization of organ pipes: experimental observations and modeling. The Journal of the Acoustical Society of America. 2006 Apr;119(4):2467-75.

[5] Okada M, Kaburagi T. Higher-order frequency locking of an organ pipe: A measurement study based on synchronization theory. The Journal of the Acoustical Society of America. 2018 Mar;143(3):1514-22.

[6] Kühnelt H, Simulating the sound generation in flutes and flue pipes with the Lattice-Boltzmann-Method. Proceedings of ISMA. 2004.

[7] Miyamoto M, Ito Y, Iwasaki T, Akamura T, Takahashi K, Takami T, et al. Numerical Study on Acoustic Oscillations of 2D and 3D Flue Organ Pipe Like Instruments with Compressible LES. Acta Acustica united with Acustica. 2013 Jan 1;99(1):154-71.

[8] Giordano N. Simulation studies of a recorder in three dimensions. The Journal of the Acoustical Society of America. 2014 Jan;135.

[9] Shi Y, da Silva AR, Scavone GP. Numerical Simulation of Whistles Using Lattice Boltzmann Methods. Proceedings of ISMA. 2014.

[10] W. S. Kam E, So RMC, Fu S, Leung R. Finite Difference Lattice Boltzmann Method Applied to Acoustic-Scattering Problems. Aiaa Journal - AIAA J. 2010 Feb;48:354-71.

[11] Tsutahara M. The finite-difference lattice Boltzmann method and its application in computational aero-acoustics. Fluid Dynamics Research. 2012 Aug 1;44(4):045507.

[12] Viggen EM. Acoustic multipole sources for the lattice Boltzmann method. Phys Rev E. 2013 Feb;87(2):023306.

[13] Tam CKW, Webb JC. Dispersion-Relation-Preserving Finite Difference Schemes for Computational Acoustics. Journal of Computational Physics. 1993 Aug;107(2):262-81.

[14] Tam CKW. Computational aeroacoustics - Issues and methods. AIAA Journal. 1995 Oct;33(10):1788-96.

[15] Zou Q, He X. On pressure and velocity boundary conditions for the lattice Boltzmann BGK model. Physics of Fluids. 1997 Jun;9(6):1591-8.

[16] Tabata R, Kobayashi T. Numerical Simulation of a Flue Instrument with Finite-Difference Lattice Boltzmann Method using GPGPU. The International Conference for High Performance Computing, Networking, Storage, and Analysis. 2018.

[17] Hejranfar K, Ezzatneshan E. A high-order compact finite-difference lattice Boltzmann method for simulation of steady and unsteady incompressible flows. International Journal for Numerical Methods in Fluids. 2014 Aug;75(10):713-46.

[18] Ghia U, Ghia KN, Shin CT. High-Re solutions for incompressible flow using the Navier-Stokes equations and a multigrid method. Journal of Computational Physics. 1982 Dec;48(3):387-411.

[19] Brown GB. The vortex motion causing edge tones. Proceedings of the Physical Society. 1937 Sep 1;49(5):493-507.